Detection of the Orbital Angular Momentum in Optics

Olivier Emile, Janine Emile, Christian Brousseau

Detection of the Orbital Angular Momentum in Optics

Olivier EMILE*

Université Rennes 1, F-35000 Rennes, France

Janine EMILE

Université Rennes 1, CNRS, IPR (Institut de Physique de Rennes) - UMR 6251, F-35000 Rennes, France

Christian BROUSSEAU

Université Rennes 1, CNRS, IETR (Institut d'Electronique et de Télécommunications de Rennes) - UMR 6164, F-35000 Rennes, France

(Dated: March 15, 2019)

Abstract

The study of Orbital Angular Momentum (OAM) of electromagnetic fields is an exponentially growing scientific field, with many potential applications. One of its key issue is the characterization, the sorting, and the detection of this orbital angular momentum. Several methods to analyze it have been developed. They can be listed in four different general technics. The first one consists in transforming the OAM electromagnetic field into a plane wave using optical elements, and then in analysing this plane wave. The second one is based on the observation of interferences fringes. These fringes arise either from the interference between the beam carrying OAM and a plane wave, or from self-interferences, or from diffraction. The third one looks for frequency shifts of a transmitted beam carrying OAM through a rotating medium using the beat frequency with an unshifted beam. It takes advantage of the so-called rotational Doppler shift. The fourth one is related to the true real mechanical nature of the OAM. It is a direct measure of the torque exerted by the electromagnetic field on an object. In this chapter, these different technics are reviewed and discussed, describing their main advantages and disadvantages, and giving key ready to use issues to detect OAM.

* olivier.emile@univ-rennes1.fr

I. INTRODUCTION

Although the ideas concerning angular momentum of light were already described in Poynting's early work [1, 2], Orbital Angular Momentum (OAM) of light has gained a tremendous renew of interest in the 90's [3, 4] and is now an exponentially growing field, because of many applications especially in telecommunications. Its main characteristic is that the Poynting vector of an OAM carrying field is spiraling along the direction of propagation. The OAM characterizes the whole beam. It is totally different from the Spin Angular Momentum (SAM) which is linked to the polarization of light. Besides, one can define the polarization on a given specific point. Then, contrarily to OAM, SAM can be defined locally.

There are many foreseen applications of the OAM. Among these applications one can note: i) Developpements in imaging technics, where OAM can reveal the helicity of a surface [5] or the sign of its curvature [6, 7] . ii) Uses in astrophysics, such as in radioastronomy [8, 9] or as an astronomical source [10], or as an optical coronagrah [11]. iii) In manipulating objects with OAM [12, 13] such as driving micromachines [14], applying torques on liquid crystals [15], or trapping and rotating particles with light fields [16, 17]. iv) In quantum entanglement [18, 19] that can be then used in cryptography, or from a more fundamental point of view in quantum mechanical problems [20–24], or performing logic quantum gates [25]. v) In material processing [26, 27] or in atom guiding due to the intensity distribution of beams carrying OAM [28–30]. However, the most discussed application of OAM is probably in telecommunication devices. Indeed, due to the orthogonality of the modes carrying different OAM, they may offer a new diversity in telecommunications, either in radio [31, 32] or in optics [33–35]. One of the key issue in all these applications and experiments is the detection of the OAM.

There have been several reviews about OAM [13, 36–41]. People were mainly interested in its generation and its use in various applications. In this book chapter we are mostly interested in the practical detection and characterization of

OAM. Such detection and characterization are key issues in the use of OAM. This chapter is organized as follow. The first section is dedicated to some theoretical background that may be useful in the rest of the chapter (section II). The following section (section III) deals with the transformation of OAM carrying beams into a fundamental Gaussian beam using optical elements. The next section reports the detection of OAM beams using interferences (section IV), either with plane waves (section IV A), or with self-interferences (section IV B) via usual interferometers (subsection IV B 1) or via diffraction (subsection IV B 2). Section V deals with the use of the so-called rotational Doppler shift to detect the OAM via frequency shifts. The last section (section VI) describes the use of the very true mechanical properties of the OAM, i.e., the angular momentum of light, to study its detection via its transfer to an object, before reaching a conclusion.

II. THEORETICAL BACKGROUND

Most of the time, a beam carrying OAM is described as a beam whose phase on a plane perpendicular to the direction of propagation is not constant. Its phase varies from 0 to $2\pi\ell$ around the beam axis (see figure 1), where ℓ is the so-called topological charge of the beam. This means that the electric field E varies as $E(r,\theta) = E(r)e^{i\ell\theta}$, where (r,θ) are the polar coordinates, in a plane perpendicular to the direction of propagation. In particular, this implies that the equiphase surfaces are no more planes, as for plane waves. They spiral around the axis of propagation, as well as spirals the Poynting vector. Moreover, there is a phase discontinuity at the beam center ($r = 0$). Therefore, the amplitude of the electric field at the origin must be equal to zero. Because of this, OAM carrying beams are also called vortex beams. This is exemplified in figure 1.

Actually there is a particular kind of vortex beams called Laguerre Gaussian beams that are mostly used in optics. The amplitude distribution of the electric

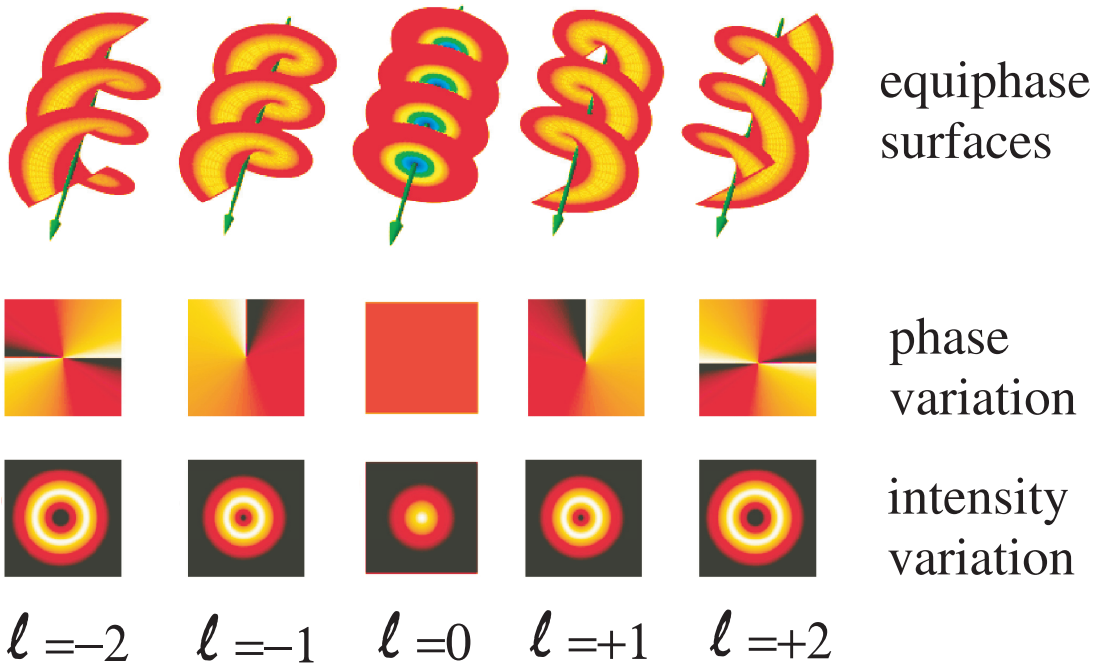

FIG. 1. Representation of beams carrying OAM. (Top): equiphase surfaces. For non zero values of ℓ, these phases are spiraling along the direction of propagation so as the Poynting vector that is perpendicular to the surfaces. (Middle): phase distribution of the electric field in a plane perpendicular to the direction of propagation. (Bottom): intensity distribution in a plane perpendicular to the direction of propagation, showing the hole in the center of the beam (vortex beam) for non-zero values of ℓ. The representations have been plotted for $\ell = -2, -1, 0, +1, +2$ topological charge. This figure is inspired from [42].

field of such beams can be written as [36, 43]

$$E_\ell(r,\theta,z) = \begin{bmatrix} \frac{C}{w(z)}\left[\frac{r}{w(z)}\right]^{|\ell|} \exp\left[\frac{-r^2}{w^2(z)}\right] \times \\ L^{|\ell|}\left[\frac{2r^2}{w^2(z)}\right] \exp(i\varphi(r,z)) \exp(i\ell\theta) \end{bmatrix}, \tag{1}$$

where r and θ are the polar coordinates, z is the distance at which we consider the beam, and $w(z)$ is the beam waist. C is a normalization constant, $L^{|\ell|}$ is the ℓ Laguerre polynomial, and $\varphi(r,z)$ is a phase term related to the propagation. The

beam waist varies with z as

$$w(z) = w_0\sqrt{1 + z^2/z_R^2} \tag{2}$$

where $z_R = \pi w_0^2/\lambda$ is the so-called Rayleigh range, w_0 is the beam waist at the origin, and where λ is the wavelength of light.

Those equations only refer to the amplitude and phase variations of the electric field. However, OAM beams are more than beams with non uniform phase variation. In a more general point of view, the angular momentum of light is characterized by a vector quantity that expresses the amount of dynamical rotation present in the electromagnetic field of the light. The density of the total angular momentum of light $\mathbf{J}$ is expressed as follows [44]

$$\mathbf{J} = \epsilon_0 \mathbf{r} \otimes (\mathbf{E} \otimes \mathbf{B}), \tag{3}$$

where $\mathbf{B}$ is the magnetic field and ϵ_0 is the vacuum electrical permittivity. $\mathbf{J}$ is nothing but proportional to the vector product of $\mathbf{r}$ and the Poynting vector $\mathbf{P} = (\mathbf{E} \otimes \mathbf{B})/\mu_0$, where μ_0 is the vacuum magnetic permeability. In most cases, this angular momentum can be separated into two terms, one corresponding to the SAM associated with the circular polarization of light and the other associated with the OAM of light. Actually, the problem of separating OAM and SAM is still a debated issue, discussed by several authors [44–47]. In particular, for example, in tightly focused beams, SAM and OAM become intermingled. They can exchange between one another [48]. OAM and SAM do not satisfy the transversality condition in the general case any more [49]. Nevertheless, within the paraxial approximation, this separation always makes sense. The purpose of this chapter is not to discuss this separation and we will assume that we can always treat beams within the paraxial approximation. Then, the SAM density $\mathbf{S}$ can be written as

$$\mathbf{S} = \epsilon_0 \mathbf{E}_\perp \otimes \mathbf{A}_\perp, \tag{4}$$

where $\mathbf{E}_\perp$ and $\mathbf{A}_\perp$ are the transverse components of the electric field and the potential vector, respectively. The OAM density $\mathbf{L}$ is

$$\mathbf{L} = \epsilon_0 \sum_{i=x,y,z} E^i(\mathbf{r} \otimes \nabla)A^i, \tag{5}$$

where the i-superscripted symbols denote the cartesian components of the corresponding vectors. It has to be noted that the sum of the OAM density and the SAM density equals the angular momentum density ($\mathbf{L} + \mathbf{S} = \mathbf{J}$). Thus OAM can be deduced from angular momentum and SAM.

The rest of this chapter is dedicated to the detection and the characterization of OAM beams, using either the amplitude and phase variations of equation 1, or the OAM density related to equation 5.

III. OAM BEAMS TRANSFORMATION

OAM beams can be transformed into plane waves, which can be then easily analyzed and identified. This can be done with lenses, spiral phase plates, or diffraction gratings. Actually, the same elements as the ones used to transform plane waves into OAM beams can be used as well.

A. Lenses

The most intuitive way to detect OAM carrying beams is to transform a vortex beam, using well characterized optical elements, into a plane wave or to any wave that can be unambiguously determined. This was indeed the first technics used to characterize OAM beams [4, 50]. The most popular way of doing it is to used two identical cylindrical lenses. Indeed, two identical cylindrical lenses with the same orientation (the curvature of the two lenses has the same orientation), separated form $\sqrt{2}f$ (f being the focal length of the lenses) transform a Laguerre Gaussian beam (that carries OAM) with a topological charge ℓ into a Hermite Gaussian

beam $H_{\ell,0}$ (that does not carry any OAM), oriented at 45° from the axis of the lenses. Then one has to identify the Hermite Gaussian beam. In particular, these Hermite Gaussian beams are characterized by ℓ zeros of intensity. So, one has to count the number of zeros of intensity to exactly determine ℓ.

One has to note that in using such two cylindrical lenses, the outgoing Hermite Gaussian beam has the same characteristics (waist, divergence) as the incoming Laguerre Gaussian beam. Such cylindrical lenses are analogous to the action on polarization of a birefringent $\lambda/4$ plate. The conversion efficiency is quite high (nearly 100%).

However, if one only wants to characterize the Laguerre Gaussian beam, one can use one cylindrical lens solely, and analyses the resulting Hermite Gaussian beam. As previously described, one has to identify the number of zeros of intensity. Nevertheless, the propagation characteristics of the Hermite Gaussian beam in this case is very different from the incoming Laguerre Gaussian beam. This can be also realized using an usual spherical lens, that can be found in every research lab, and tilting it, regarding to the propagation axis. This introduces astigmatism, and the lens is equivalent to a cylindrical lens [51, 52]. An example is displayed on figure 2. The main advantage of these two technics is that they are relatively cheap and they can be used for any optical wavelength.

Analogously, one can also use technics that generate OAM carrying beam from plane waves, and reverse it, to transform back OAM beams into plane waves. For example, one can reverse a spiral phase plate [53] to transform a Laguerre Gaussian beam with a well-defined topological charge ℓ into a plane wave. Figure 3a shows an example of such a spiral phase plate. Although this particular example has been used in the radio domain [54, 55], the principle remains the same as in optics. Actually, the characteristics of the elements used to transform OAM beams into plane waves in the radio domain, such as phase plate, have geometrical dimensions of the order of the wavelength or higher (i.e. in the centimeter range).

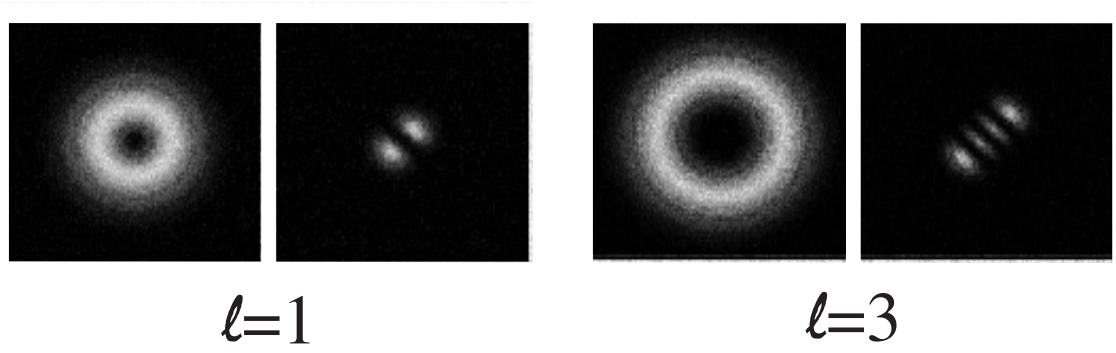

FIG. 2. Experimental transformation of a Laguerre Gaussian beam (left part) with $\ell = 1$ and $\ell = 3$ in a Hermite Gaussian beam (right part) using a single spherical lens. This spherical lens is tilted by 20° around the vertical axis. The number of zero of intensity of the Hermite Gaussian beam is equal to 1 and 3, corresponding to $\ell = 1$ and $\ell = 3$ respectively. This enables to clearly identify the topological charge of the Laguerre Gaussian beam.

Their principle can be better visualized. They can be checked with the naked eye. This is the reason why we decided to present such elements in figure 3.

The thickness of the plate varies linearly with the azimuthal angle. Then the phase difference for two different azimuthal angles depends on the thickness difference. For a 2π variation, the phase difference must be equal to $kne(\theta) = 2\pi\ell$, k being the wave vector, n the optical index, and e the thickness of the plate. Of course a spiral phase plate is only dedicated to a given wavelength. Nevertheless, it can also be used for twice the wavelength (assuming a constant optical index), for generating twice the topological charge, or even an integer multiple of the initial wavelength. Figure 3b shows an alternative to such spiral phase plate, where n (due to the drilling of holes in the material) is varying linearly with the azimuthal index. The phase difference condition is $kn(\theta)e = 2\pi\ell$. Such a plate also corresponds to a given wavelength only.

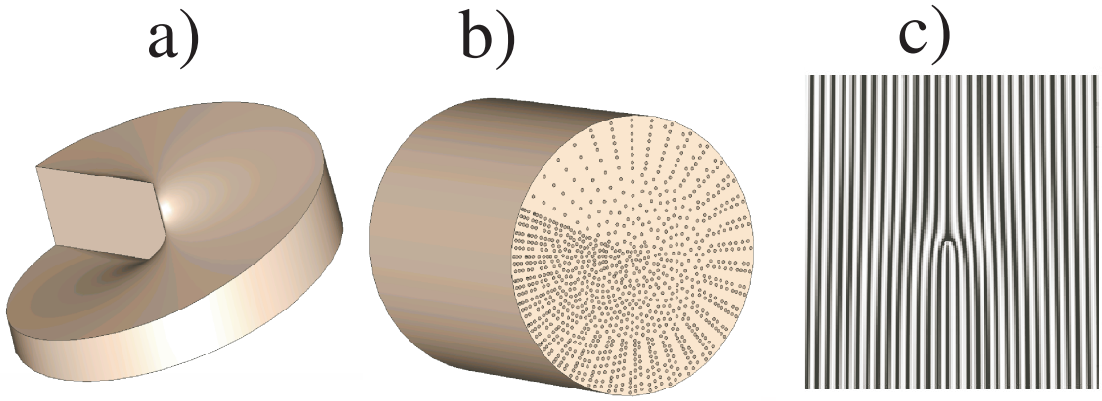

FIG. 3. Optical elements used to transform OAM beams into plane waves a) Spiral phase plate. The height of the plate varies with the azimuthal angle. Thus the phase of the outgoing beam has a non uniform phase. b) Azimuthal index variable plate. Because of the drilled hole the optical index varies with the azimuthal angle. A detailed description of the plate can be founded in [55]. It has to be noted that a similar technics can be transposed in optics using an index varying material. c) Forked diffraction grating for a $\ell = 2$ Laguerre Gaussian beam. It results from the combination of a helical phase distribution profile with a linear phase ramp. Note that such a forked grating can be readily printed on a transparency and put in front of a beam. For a fundamental Gaussian incoming beam, the first diffraction order corresponds to a $|\ell| = 2$ beam. Conversely, for a $|\ell| = 2$ incoming beam, the first diffracted order outgoing beam is a plane wave.

B. Grating

However, perhaps the most easier way to transform OAM beams into plane waves is via hologram or forked diffraction gratings [3, 56, 57] . An example of such a grating is presented in figure 3c, for a $|\ell| = 2$ topological charge. Such gratings can be readily printed on a transparence sheet, or alternatively a Spatial

Light Modulator (SLM) [34, 58] can be used in order to compute reconfigurable holograms. Such gratings are to some extend wavelength independent. For example, for a forked grating corresponding to a topological charge equal to $|\ell| = 2$, if the incoming beam has a component $|\ell| = 2$, then first order diffracted outgoing beam would be a plane wave.

So far, the transformation of a Laguerre Gaussian beam into a plane wave or into a Hermite Gaussian beam is adapted for vortex beams with well-defined topological charges, because the optics for the transformation are dedicated to a single topological charge. In the case of a superposition of several Laguerre Gaussian beams, the use of optics to transform OAM beam as described here is more tricky. Indeed, the outgoing beam has a fundamental Gaussian beam component, for a given optics of transformation, but also several higher order Laguerre Gaussian beams.

Nevertheless, one can use several such optics in parallel to transform vortex beams into a superposition of several beams, with one of them being a plane wave, or equivalently a fundamental beam (with $\ell = 0$). In order to select the intensity corresponding to the pure fundamental Gaussian beam, one can collimate the total output beam into a fiber. The fundamental beam is the only mode that couples efficiently to the fiber. The spatial extension of the other modes is indeed to large. They suffer high losses.

Then, placing a detector at the end of the fiber enables to identify the amount of light coupled into the fiber (which is indeed the fundamental beam), and thus the proportion of the beam corresponding to a given topological charge, for a given optics, with a well-defined mode transformation. If the detector is a high-quality photodetector (i.e. a detector with a high quantum efficiency giving one electron for one incoming photon such as avalanches photodiodes or photomultipliers), the detection could be performed even with low output powers.

Because each detection systems measures only one mode at a time, in order

to ensure a complete analysis, the initial beam has to be split in several parts, transformed and then analyzed with a fiber and a detector dedicated for a given topological charge. It turns out that the efficiency of such an approach is limited to $1/N_\ell$, where N_ℓ is the number of topological charges to be assessed [18, 59]. This technics has been for example implemented for telecommunication purposes using a phase mask, that is equivalent to a spiral phase plate [33, 60]. More complicated holograms can be designed, where the different input modes generate fundamental Gaussian beams in different orders of the grating [34, 61–63]. However, the principle remains unchanged.

IV. INTERFERENCES

The principle of superposition is at the very basis of interferometry. It combines waves in a way that the result of their combination (interference patten) leads to some properties (number of interferences, shapes of the interferences) used as a diagnostic of the original state of the waves (phase variation, topological charge, ...). When two waves with the same frequency combine, the resulting intensity distribution or pattern depends on the phase difference between the two waves. Waves that are in phase will undergo constructive interference while waves that are out of phase will undergo destructive interference. Waves which are not completely in phase nor completely out of phase will have an intermediate intensity pattern, which can be used to determine their relative phase difference [64, 65].

Since a vortex beam has a non-uniform phase variation, the best way to characterize this phase variation is thus probably via interferences. The beam to be analyzed could interfere with a plane wave, as described in the next paragraph (subsection IV A), or with self-interferences that will be dealt with in paragraph IV B. This last paragraph will also include discussions about interferences due to diffracting systems.

A. Interferences with plane waves

Actually, a helically phase beam interfering with a plane wave reveals phase information about the vortex beam structure and produces a spiral interference pattern with several fringes [66–68]. More precisely, looking at the phase term only, the intensity distribution and thus the interference pattern should vary with the azimuthal angle θ as

$$|1 + e^{i\ell\theta}|^2 \sim 4\cos^2(\frac{i\ell\theta}{2}) \tag{6}$$

This corresponds to a modulation of the intensity with θ. In a plane, using polar coordinates, the bright and dark fringes are straight lines originating from the center of the vortex corresponding to a given value of θ. One has to count the number of fringes to determine the exact topological charge. This is the ideal case of a vortex beam that is collimated. If the vortex beam is converging or diverging, one as to take into account the extra propagation length when projected on a plane perpendicular to the direction of propagation (the $\exp[i\varphi(r, z)]$ term in equation 1). Then the fringes are still originating from the center but also spiral, as can be seen in figure 4.

Waveform and phase information can also be recovered from a Shack-Hartmann method [69]. This method is based on a wave front sensor technics. More precisely, an array of small lenses focus a collimated beam into a corresponding array of spots. The displacement of each individual spot, measured with a CCD camera, is proportional to the tilt of the local wavefront of the beam at that point. Then, the resultant tilt measurement is integrated over the discrete set of points in order to recover complete phase information. It has been shown that this commercially available Shack-Hartmann wave front sensor can characterize OAM beams as well [70–72]. Nevertheless, the goal of such a technics, as for the interference with a plane wave is to recover the phase information about the vortex beam.

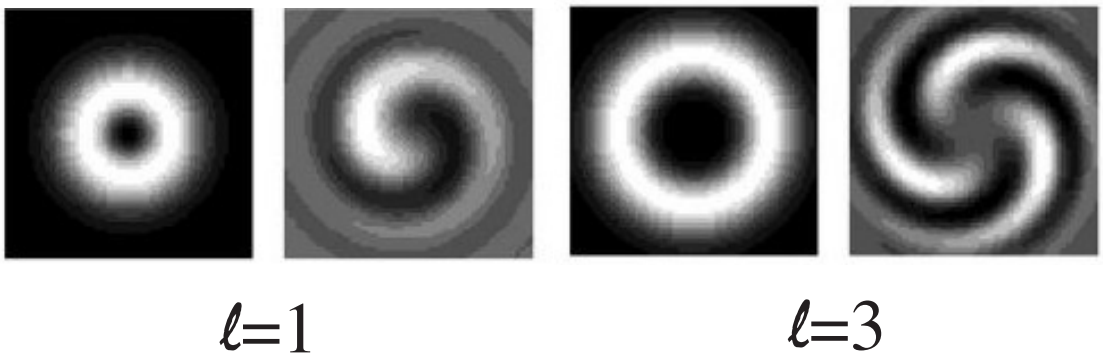

FIG. 4. Experimental interference (right) of a Laguerre Gaussian beam (left) with a plane wave for $\ell = 1$ and $\ell = 3$ Laguerre Gaussain beams respectively, showing the spiraling structure. The Laguerre Gaussian beams are here slightly diverging.

B. Self-interferences

Self-interferometers can be divided in two main domains: wavefront splitting interferometers, and amplitude splitting interferometers. A wavefront splitting interferometer divides a wavefront emerging from a point or a narrow slit in different parts. After allowing these parts to travel through different paths, they are recombined, and they then interfere. An amplitude splitting interferometer divides the amplitude of the incident wave in two parts with a partial reflector. Half of the intensity is transmitted, the other half is reflected. The two separate beams, after propagation are then recombined, before interfering. Both interferometers can be used to characterize OAM beams.

1. Amplitude splitting interferometers

Amplitude splitting interferometers refer mainly to Mach-Zehnder, Michelson, and Fizeau interferometers. They are all based on the same principle. The initial beam is split in two parts, one of them suffers a topological phase modification

before being recombined with the other part. Mach-Zehnder interferometers have been used to perform interferences between Laguerre Gaussian beams and plane waves. Indeed, an optical element transforms the Laguerre Gaussian beam into a plane wave. This leads to the interference between a vortex beam and a plane wave [67, 73]. The resulting interference pattern is analogous to what have been described in the previous subsection (subsection IV).

When one considers the interference of a beam with itself, the whole beam experiences the same extra phase variation. The result is analogous to what can be obtained with a plane wave. It may provide information on a phase difference in one arm of the interferometer, but hardly gives any information on the phase of the beam itself.

Nevertheless, if one reverses the initial topological charge ℓ in one arm of the interferometer by adding a dove prism, a corner cube instead of a mirror, or a cylindrical lens, the interference will become interference between an OAM beam with a ℓ topological charge and an OAM beam with a $-\ell$ topological charge [19, 74, 75]. This technics is used for example in quantum information [18, 76, 77], or in rotational Doppler measurements [78, 79]. Considering the phase term only, the angular intensity variation is simply described by

$$I(\theta) = |e^{i\ell\theta} + e^{-i\ell\theta}|^2 \sim 4\cos^2(l\theta) \tag{7}$$

In polar coordinates, this corresponds to straight lines originating from the center of the vortex, whatever the converging nature of the beam. Besides, one has to take into account the variation of the intensity with the distance to the center of the vortex, which is much more important than for interferences with a plane wave as described in the previous paragraph. Then, the interference pattern corresponds to a daisy flower [24, 80] as can be seen in figure 5. The number of petals is exactly twice the topological charge ℓ. One has just to identify the number of petals to characterize the vortex beam.

This technics can be used even with very high values of the topological charge.

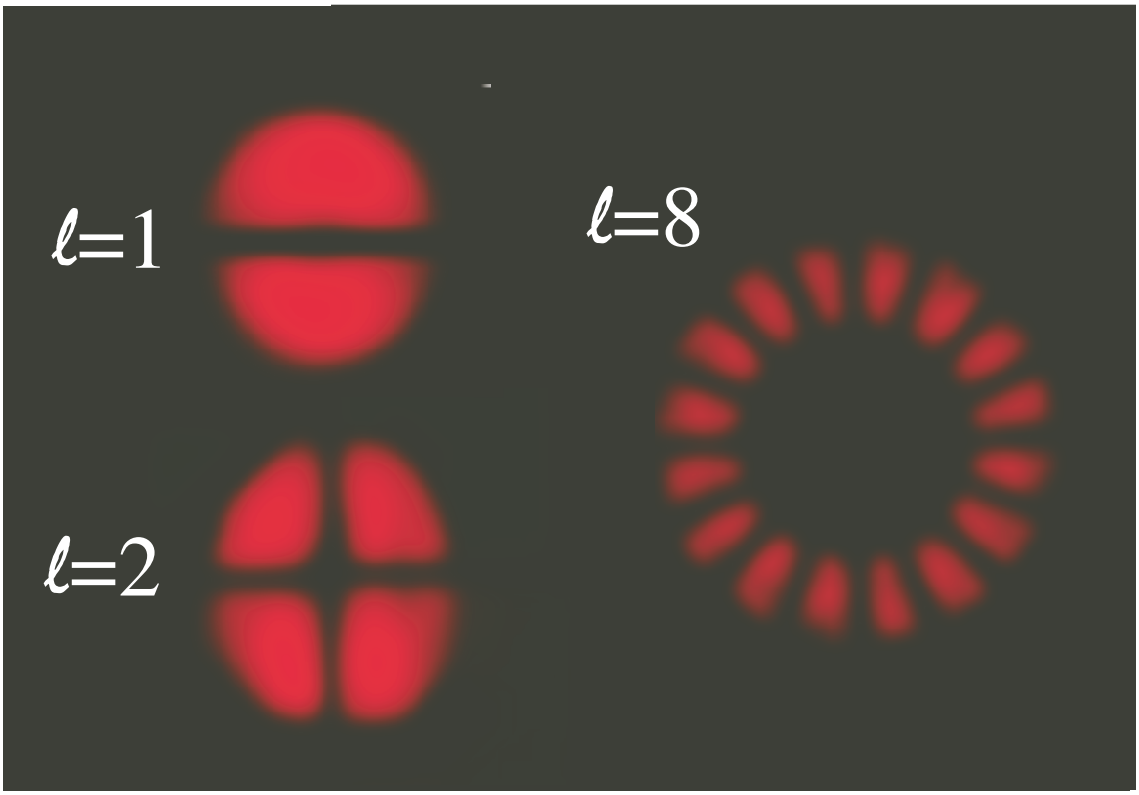

FIG. 5. Examples of interference patterns at the output of a Michelson interferometer. They indeed correspond to the interference between opposite topological charges ($\ell = +1$ and $\ell = -1$, $\ell = +2$ and $\ell = -2$, $\ell = +8$ and $\ell = -8$). It exemplifies the daisy flower like interference pattern.

Indeed patterns with $\ell = 10010$ have been recently observed [81] and used in quantum entanglement experiments. Such high values of ℓ is of crucial importance. Actually, it is often believed, according to Bohr correspondence principle, that the transition between quantum and classical worlds transition occurs when the quantum number of the investigated state becomes very large. Such high values of ℓ, that corresponds to the topological charge ℓ quantum number, show that such belief is incorrect.

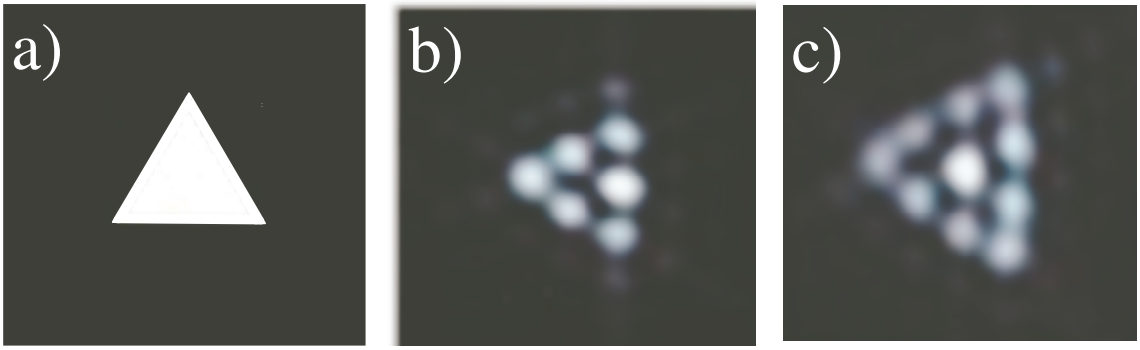

FIG. 6. Diffraction by an equilateral triangular aperture a). b) and c) Experimental pictures of diffraction patterns for a $|\ell| = 2$ and $|\ell| = 3$ topological charge, respectively, obtained on a screen and observed with the naked eye. The topological charge can be readily identified on the picture. It corresponds to the number of dark periods on the side of the triangular pattern. Note that the orientation of the triangular pattern is rotated by 90° regarded to the triangular aperture.

2. Wavefront splitting interferometers

In a wavefront splitting interferometer, the light emerging from a point or a slit is divided, propagates freely and then recombines on a detector or on a screen. Among the various wavefront splitting methods that have been developed to detect OAM, the most popular one is the diffraction by a triangular aperture [82–85]. The question of the diffraction of a plane wave by a triangular aperture from a theoretical point of view has been considered some times ago [86]. However its application to an OAM beam can only be solved by simulations. Nevertheless, experimentally, the diffraction pattern is a collection of spots within a triangle, as can be seen on figure 6. The number of spots on the triangle side equals $\ell + 1$. One has only to consider the number of spots to fully characterize the Laguerre Gaussian beam.

It has to be noted that the angle between the orientation of the diffraction tri-

angle and the triangle corresponding to the repartition of the spots always equals 90°. Most importantly, such a technics enables to discriminate between opposite topological charges. For example on figure 6, the triangle corresponding to the diffraction pattern points towards the left. An OAM beam with a reversed topological charge would have pointed towards the right. People have been able to measure topological charges up to $|\ell| = 7$, but the experiment becomes tricky after this value [84], because the different spots overlap.

The other useful technics to characterize OAM beams with wavefront splitting interferometers relies on Young's double-slit experiment [87–90]. The well-known straight lines which are characteristic of Young's double-slit interference pattern experiment are then replaced by twisted lines, as can be seen in figure 7. The shape and the twist of the fringes can be calculated exactly. For example, for a $\ell = 1$ topological charge, they follow a -2 $\tan^{-1}(a/z)$-variation, where z corresponds to the vertical axis and where a is half the distance between the slits. The interferences, at the bottom zone of the laser beam, have been shifted by exactly one interference order compared with the ones corresponding to the upper zone of the laser beam (see green arrows on the figure 7b). The only condition to obtain such a pattern is that the separation between the two slits is much smaller than the radius of the vortex beam, in order to probe the whole beam. Otherwise, the fringes are truncated.

As l is further increased, the twist of the fringes becomes more and more important. For $l = 2$, the fringes at the bottom zone (see figure 7) have been shifted by two interference orders compared to the ones at the upper zone, whereas for $l = 3$ they correspond to three interference orders. Analogously, for $l = n$, they should correspond to n orders. However for $\ell \geqslant 7$, the fringes become difficult to identify. In particular, the fringes mix together especially in the center of the interference pattern that corresponds to the central part of the vortex beam where the intensity is rather low.

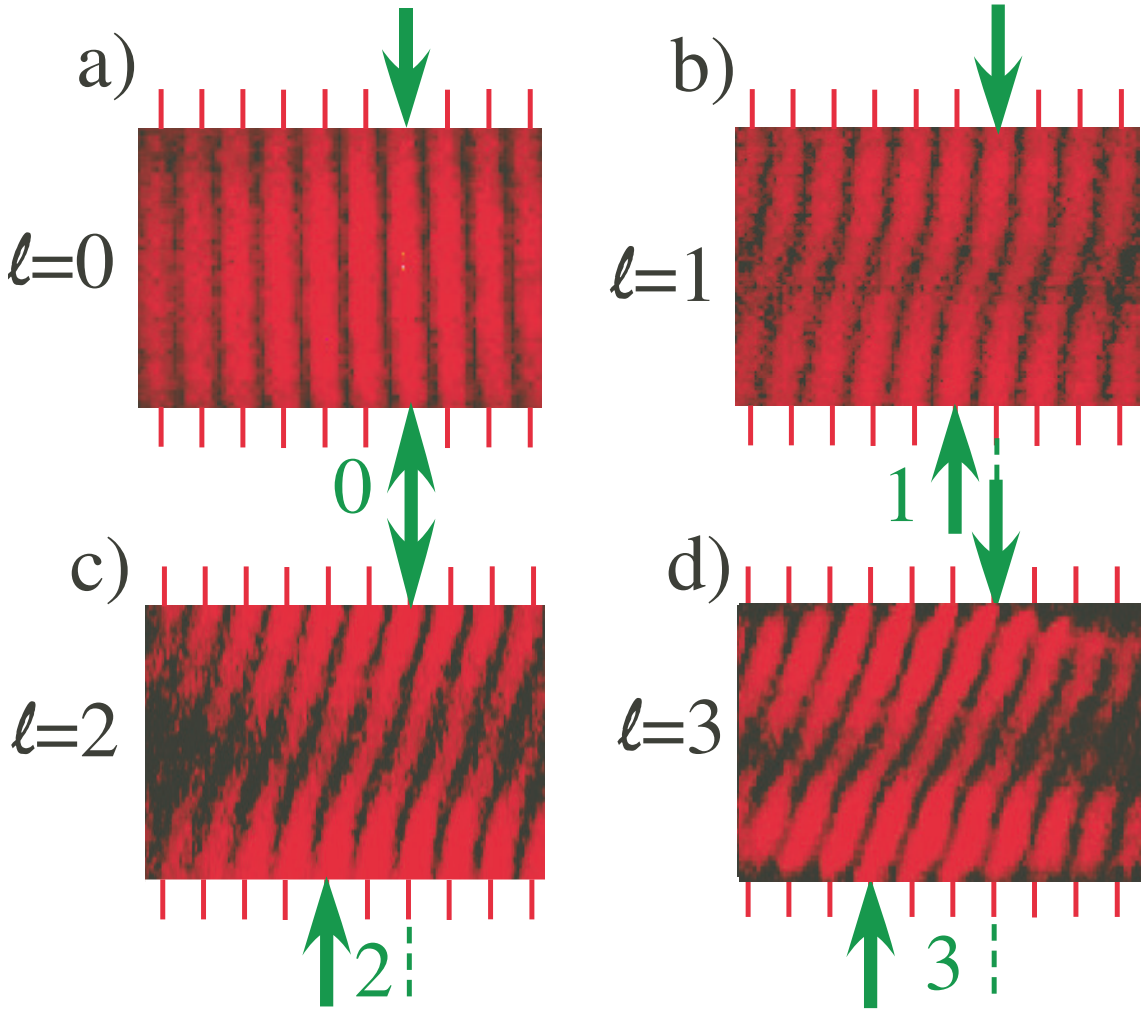

FIG. 7. Young's double slit interference: twisted interference patterns for beams with a) $l = 0$ (usual double slit interference pattern); b) $l = 1$; c) $l = 2$; d) $l = 3$, for a vertical double slit orientation. The twist corresponds to l bright fringes of the interference pattern. The green arrows indicate the fringe order shift. From the twist, one can unambiguously determine the topological charge.

As the sign of the topological charge is reversed, the fringes are shifted in the other direction. As for the triangular aperture technics, Young's double slit experiment technics enables to discriminate between topological charges of opposite

values. Such experiment can be easily performed since there is always a double slit set up in every experimental physics lab, otherwise, it is easy to implement.

Similar results can be obtained with set-ups that are equivalent to Young's double-slit experiment as with Fresnel bi-prism for example [91]. Some experiments dealt with dynamical double-slits [92, 93], others use angular double-slits [94]. In particular, they have been able to recover the topological charge of a Laguerre Gaussian beam in the periodically varying far field interference pattern direction of the angular double-slit experiment. This is also valid for fractional topological charges. Some use single slit [95, 96] where the interference patterns bend due to the phase variation. Others use an iris diaphragm [97] to produce ball bearing sorts of structure of darkness and brightness, or an annular aperture [98] that leads to alternate bright and dark rings. However, the principle of the experiment and of the detection remains roughly the same.

There is perhaps one last method among the various wavefront splitting interferometers that is worth to be noticed, since it can be used to sort or demultiplex OAM beams. It relies on multipinhole interference [99–101]. Briefly, the OAM beam is analyzed with a hole-wheel, with holes regularly drilled on the wheel at a constant distance from the center. As the topological charge is a multiple of the number of holes, the diffraction pattern is identical to the diffraction pattern generated by a plane wave. This pattern can be unambiguously identified using an ordinary photodiode on the axis (see figure 8).

V. ROTATIONAL DOPPLER SHIFT

Up to now, the technics described in this chapter aim at identifying the phase variation of the beam. This phase variation is linked to the OAM of light. Nevertheless, the information is rooted into the phase. A phase variation does not give any direct information about the *angular momentum* of light and thus on the true

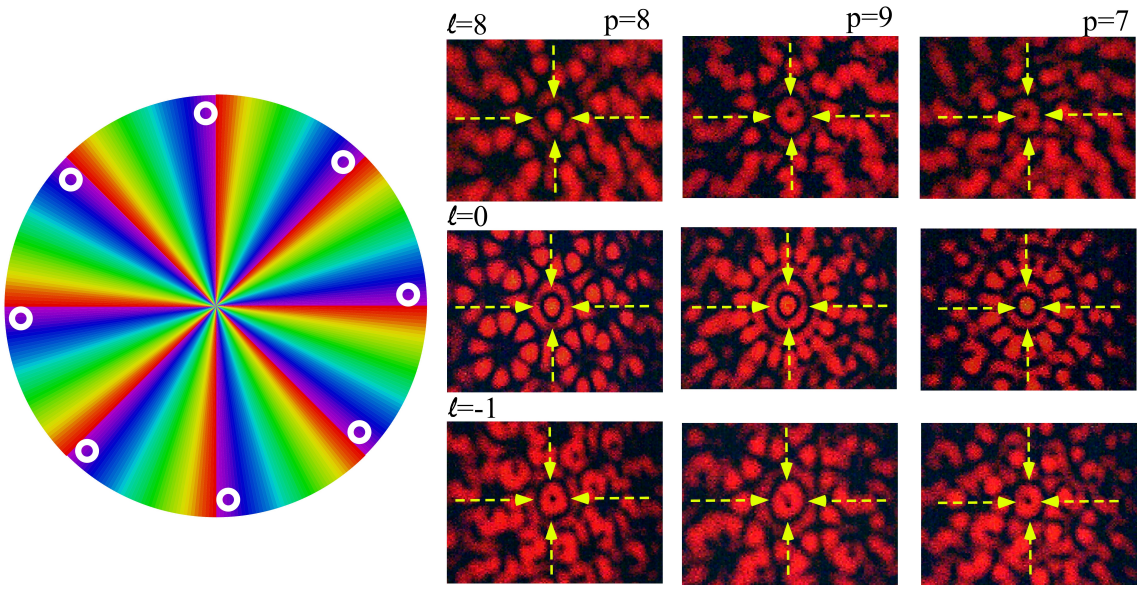

FIG. 8. Principle of the hole-wheel measurement. Left: phase distribution of the OAM beam and coincidence of the holes. Right: interference patterns with different values of the topological charges ℓ and for different values of the number of holes p. Only when the topological charge is a multiple of the number of holes ($\ell = np$, n being an integer), the pattern is the same as the one obtained with a plane wave. In particular, the center of the pattern corresponds to a bright spot whereas for the other it corresponds to a dark spot.

value of the OAM carried by the light beam.

On the other hand, an object in rotation (a spinning object) can modify the characteristics of a beam carrying OAM. Indeed, the light frequency is changed due to the so-called rotational Doppler shift [78, 79, 102–105]. This rotational Doppler frequency shift can be understood on the basis of the linear Doppler shift [79]. In particular, the helical phasefront of a Laguerre Gaussian beam corresponds to a local skew angle of the Poynting vector (or local ray direction of light) of $\alpha = \ell/(kr)$. Let us recall that k is the wave vector and r is the radius vector with respect to the axis of the beam. This angle is small compared with 1. Consequently,

for a point at a distance r and a velocity v on a surface spinning with an angular velocity Ω ($v = \Omega r$), the variation of the light pulsation due to the (usual) Doppler frequency shift $\Delta\omega$ equals

$$\Delta\omega = kv \sin\alpha = k\Omega r \frac{\ell}{kr} = \ell\Omega \tag{8}$$

More precisely, the difference frequency Δf between the ingoing and outgoing beams is equal to

$$\Delta f = (\Delta\sigma + \Delta\ell)\Omega/2\pi \tag{9}$$

$\Delta\sigma$ is the SAM variation and $\Delta\ell$ is the OAM variation between the ingoing and the outgoing beams. We note that, unlike the linear Doppler shift, this angular Doppler shift is independent of the frequency of the incident light. Besides, as one can notice, it is also valid for the SAM [106–108]. One has to take care that the signs of the SAM and the OAM must be defined with respect to a given fixed axis and not with respect to the propagation or the detection direction axis, as it is usually done.

It is not so obvious to detect this frequency shift. In the radio domain, this can be easily performed using a spectrum analyzer [109, 110]. The spectrum analysis reveals several peaks. They correspond to the decomposition of the incoming beam onto a set of Laguerre Gaussian modes centered on the rotation axis. It gives a direct decomposition of the beam in this basis (including the component of the beam amplitude in a given mode that corresponds to the peak amplitude). The mode with a frequency shift that equals $\ell\Omega/2\pi$ corresponds to a topological charge that equals ℓ, ℓ being a positive or negative integer.

The frequency shift cannot be detected in optics using an optical spectrum analyzer nor a Fabry-Perot analyzer, since these analyzers do not have enough resolution to detect shifts of the order of hundreds of Hertz at most, which is typically the upper limit of the rotating frequency of the object. An other technics must be used. With SAM, this shift can be rather easily detected. Indeed, if one

combines the frequency shifted beam with a non frequency shifted beam with the opposite circular polarization, this leads to a rotating linear frequency [111]. This gives a modulation of the received intensity [106–108], that can be easily detected. The opposite circular polarization beam can also experience a rotational Doppler shift. This shift will have the opposite sign and the modulation intensity frequency will be double.

The same technics has been used for OAM. Indeed, if one combines an OAM beam with a given topological charge and a frequency that have been shifted, with an unshifted beam with a reverse topological charge, the resulting interference pattern is a rotating daisy flower which rotating frequency depends on the shift. This interference technics, that transposes the optical frequencies difference in the very low frequency range (of the order of several Hertz) has been performed in radio [112, 113] as well as in optics [78, 79, 114, 115]. This rotating or beat frequency can then be readily detected, even with a naked eye, or a usual photodiode and an oscilloscope. When several OAM modes are present, a spectral decomposition of the detected intensity (in the low frequency range) leads to the identification of the various modes. As for SAM, one beam only or the two beams with opposite charges may experience rotational frequency shifts. The beat frequency will vary accordingly.

It has to be noted that all the rotational Doppler shifts have been performed either in transmission through a rotating element (such as a Dove prism that reverses the topological charge) or looking at the diffused light upon reflection on a rough surface. It cannot be detected in reflection in principle [116]. Actually, regarded to the direction of propagation (or the direction of detection) of the SAM beam or the OAM one, the circular polarization or the topological charge is reversed. However, when the direction for the identification of the sign of the topological charge (or polarization) is fixed, there is no change of the sign. Then, looking at equation 9, there should be no rotational Doppler shift.

VI. ANGULAR MOMENTUM TRANSFER MEASUREMENTS

The rotational Doppler effect is a very nice and clever way to detect spinning object. It is based on the rotational structure of the OAM beam, and on the fact that the Poynting vector is spiraling along the beam axis. The frequency analysis of the outgoing beam leads to a complete decomposition of the incoming beam into a set of Laguerre Gaussian beams. Nevertheless, the estimation of the rotational Doppler shift is an indirect technics with respect to the OAM. Indeed it does not directly measure the OAM of the beam. This can only be performed via the angular momentum transfer illustrated by torque measurements.

A. Spin angular momentum

The first report on angular momentum transfer was performed by Beth in optics using SAM transfer [117, 118]. SAM can induce rotation of an absorbing material or a birefringent plate, for example. Indeed, a circularly polarized photon changes its helicity when passing through a half-wave plate. Then $2\hbar$ momenta are exchanged upon interaction. However, the effect is so tiny that Beth used parametric amplification to evidence rotation. Since the torque is proportional to the wavelength, it is easier to evidence the effect in the radio domain [119, 120], where absorption is the transfer mechanism. Nevertheless it is more difficult to perform quantitative measurements using microwaves. Quantitative measurements in optics, in the infrared part of the spectrum, enable the direct observation of the angular acceleration due to SAM transfer [121] (see figure 9).

In order to isolate the uniform rotation, the experiment is performed under vacuum conditions. The laser power is 10 W. The incoming polarization is chosen thanks to a quarter wave plate. The outgoing light is retro-reflected and the polarization flipped by another quarter wave plate that is crossed twice by the light field. Each photon leads to $4\hbar$ momenta exchange with the plate. Since the number

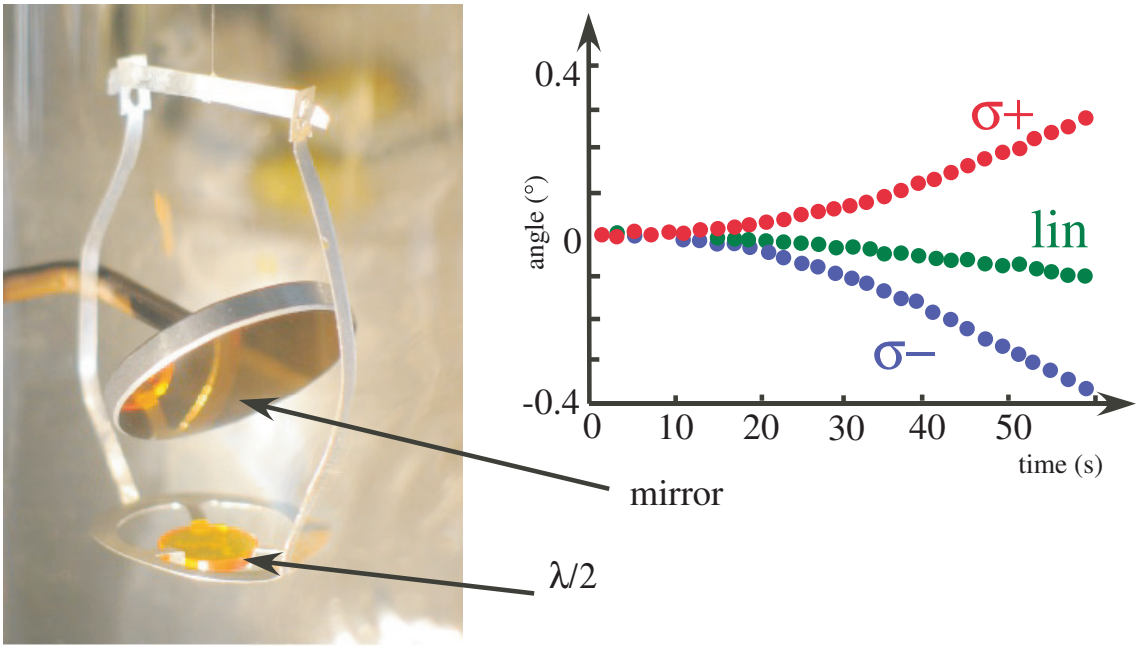

FIG. 9. Left: picture of the experimental set-up used to evidence the transfer of SAM to a halfwave plate. Right: uniform acceleration of the plate for a 10 Watts circularly right, circularly left and linearly polarized CO_2 laser.

of photon depends on the optical power, one finds that the acceleration varies linearly with the power of the outgoing field, as expected. This is a quantitative measurement of the torque applied on the plate by the SAM laser beam.

There have been other observations of the transfer of SAM to objects. In particular it has been shown that a SAM carrying beam can make small birefringent particles to rotate [122–125]. This has also been evidence on absorbing micrometer-size particles [126]. However, in these later cases, the steady state rotation only is observed. In order to deduce the torque transfer by the SAM beam, one has to estimate the friction coefficient. It depends on the liquid viscosity, on the shape of the particle, on the temperature, and whether the particle is immersed or not. This deduction is not straightforward.

B. Orbital angular momentum

The rotation of small particles (from few micrometers to a fraction of millimeter) has also been performed using OAM [16, 17, 127]. The particles were able, either to follow a trajectory around a circle which center corresponds to the axis of the OAM beam, or to spin around their own axis. Sub-millimeter objects have even been shown to rotate under the influence of the OAM light that originates from a plane wave diffracted by a non-symmetrical object [90, 128, 129]. Nevertheless, the transfer mechanism is most of the time by absorption of light carrying OAM. However, a Dove prism or a corner cube in reflection could be the equivalent for OAM of a half wave plate for SAM. One could then imagine to evidence the rotation of such objects. Nevertheless Dove prisms or corner cubes cannot be considered as small particles. Since the total angular momentum is conserved, particles must rotate. As for SAM, only the steady state rotation is observed. Then, it is difficult to precisely determine the torque. In particular, the damping coefficient has to be precisely defined as mentioned in the preceding paragraph (subsection VI A).

The transfer to a macroscopic object (in the centimeter range) has been only recently observed. It was done in the radio domain using a so-called turnstile antenna [130] (see figure 10). The emitted wave is a "2D-spherical" wave that carries OAM, in the plane of the antenna, with a topological charge equal to $\ell = 1$ or $\ell = -1$. Indeed, in the plane of the antenna (i. e. in the horizontal plane), the electric field intensity is a spherical wave, whereas in the direction perpendicular to this plane, the beam is circularly polarized. A suspended copper ring that is in the plane of the antenna, is the rotating object. The uniform rotating acceleration is evidenced. The sense of rotation is reversed when the sign of the topological charge is reversed.

A detail description of the transfer mechanism [131, 132] links the measured mechanical torque Γ, to the radiated power P and to (the topological charge) ℓ.

FIG. 10. Left: picture of the experimental set-up showing the turnstile antenna at the center of the rotating ring. The whole experiment takes place in an anechoic chamber. The radius of the ring is 15 cm. Right: principle of the experiment in order to exemplify the picture.

Actually the following relation was evidenced

$$\Gamma = \ell\hbar\frac{P}{h\nu} = \ell\frac{P\lambda}{2\pi c} \tag{10}$$

Here ν is the frequency of the electromagnetic field in the radio domain ($\nu =$ 970 MHz), λ is the electromagnetic field wavelength, $\hbar = h/2\pi$ is the reduced Plank constant, and c is the velocity of light. $N = P/(h\nu)$ is nothing but the number of photon received on the ring per second. Then the measurement of the torque, the incident power, and the wavelength lead to the determination of the topological charge (including its sign that is the same as the sign of the torque). Such measurements have also been performed using acoustic waves [133], following theoretical suggestions [134, 135] on four-panel transducers and the corresponding acoustic field. This has then been done in optics [24, 136], using an absorbing black paper hold by a cotton thread in a vacuum chamber (see figure 11). The result of equation 10, whatever the wavelength, is that ℓ is always an integer number.

Concerning The experiment performed in optics, the measurent of the incoming

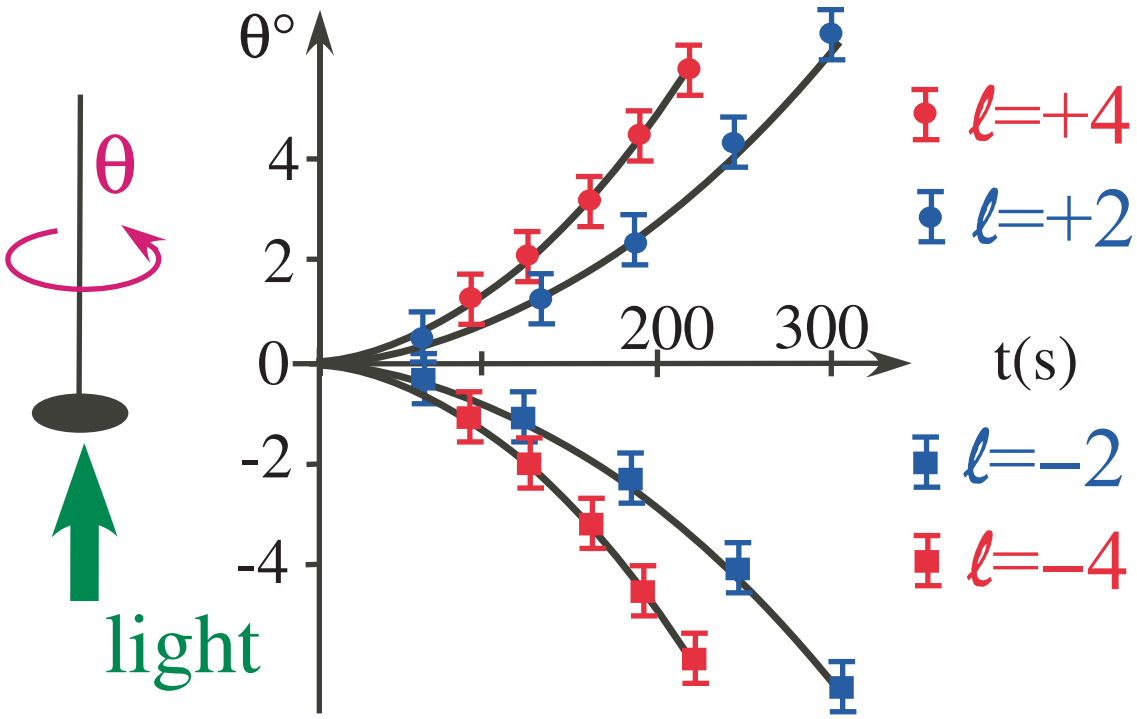

FIG. 11. Left: principle of the experiment to measure the torque induced by light in the visible domain. A black paper disk absorbs OAM light. It starts to rotate under its influence, due to the angular momentum conservation. Right: measurement of the uniform rotating acceleration for various values of the topological charge ℓ, for a 0.5 mW He-Ne laser.

power has to be performed at the place of the paper disk. This power has to be in the milliwatt range, in order not to burn the paper. The axis of the OAM laser beam has to be precisely aligned with the rotation axis in order to avoid unwanted torque effects. The experiment is thus rather tricky, however, it gives the correct value of the topological charge using the OAM transfer from light to a suspended object. It fully characterizes the OAM nature of the vortex beam.

C. Light quantization.

From a purely mechanical point of view, as reported by Truesdell [137, 138] on discussions between Euler and Bernoulli, angular momentum is a physical observable in its own right. It is independent of, and not derivable from energy measurements. The knowledge of the energy quantity does not imply the knowledge of the angular momentum and vice versa. Energy on one side and angular momentum on the other side are indeed truly independent quantities.

Let us now have a closer look at equation 10. The ratio of the measured torque times the pulsation of light, to the light power equals the topological charge, which is an integer number. This equation has been experimentally verified. The topological charge ℓ is thus quantized. One can then divide the torque by the topological charge and by the quantum of action $\hbar$. It equals N the number of photons. Then the torque and power measurements together are an experimental proof of the light quantization. This reasoning is very similar to the one performed by Raman and Bhagavantam [139] in the case of polarization.

One can nevertheless argue that when considering a classical light field with cylindrical symmetry, or equivalently with a given topological charge, one would get the result of equation 10. It seems then that there is no need to invoke any quantization of the light field. However, considering a cylindrical symmetry or a given topological charge, means that after one turn around the axis of propagation of light, the phase variation must be unchanged. It must be equal to integer number (the topological charge) times 2π. This is the continuity condition. Nevertheless, people following this reasoning implicitly assume that the OAM is quantized.

VII. CONCLUSIONS

As a conclusion one can now try to answer the question asked at the very beginning of this chapter: "From a practical point of view, what is the best way to

detect OAM in optics?" Of course, one could answer that it depends on the purpose of the detection perfomed. If one looks for a quick way to check the OAM nature of the beam, the use of a twisted cylindrical lens is the most appropriate (section III A). If one wants to determine also the sign of the topological charge, interference technics using either the diffraction by a triangular aperture or by the double-slit experiment are well adapted (section IV B 2). To perform demultiplexing of superposed beams with different topological charges, one would prefer the use of diffraction gratings coupled with an optical fiber (section III B). The Doppler effect will lead to a precise modal decomposition that may be useful to completely characterize a complex vortex beam (section V). Finally, the torque measurement indeed measures the OAM quantity carried by an OAM beam (section VI). It is a full characterization of the OAM beam and of the mechanical character of the OAM. However, this last technics is not easy to implement. Indeed a versatile and ready to use apparatus that can measure the light power and the torque is lacking.

There are many foreseen applications of OAM beams in the optical domain [40, 140–143]. One the most highly debated is in telecommunications applications. However, telecommunication systems only use the orthogonality between the modes. It is a derivative of so called MIMO (Multiple Input Multiple Output) technics. This particular system that uses OAM, shares a common symmetry axis and a common direction of propagation for all the modes [144–146]. However, they do not exploit the real OAM mechanical nature of light at all. This restriction also applies for applications in quantum cryptography which exploits the quantum nature of the OAM as well as the orthogonal properties between modes. We believe that the future of OAM relies on the rotational properties of the vortex beam that can be used to detect the rotation itself with high accuracy, or to rotate or manipulate objects, particles or atoms. In particular, such rotation manipulation could be performed without mechanical contact, even in remote areas, with extreme vacuum or temperature conditions. Alternatively, such beams carrying

OAM can be used in the detection or rotating systems, also in remote areas, using either torque or rotational measurements.

---

[1] Poynting J. H. (1909), Proc. R. Soc. London, Ser. A **82**, 560.

[2] Jackson J. D. (1975) Classical Electrodynamics, 2^d Ed., Wiley, New York.

[3] Bazhenov V. Y., Vasnetsov M. V., and Soskin M. S. (1990), JETP Lett. **52**, 429.

[4] Allen L., Beijersbergen M. W., Spreeuw R. J. C., and Woerdman J. P. (1992) Phys. Rev. A **45**, 8185.

[5] Torner L., Torres J. P., and Carrasco S. (2005), Opt. Express **13**, 873.

[6] Bernet S., Jesacher A., Fürhapter S., Maurer C., and Ritsch-Marte M. (2006) Opt. Express **14**, 3792.

[7] Ritsch-Marte M. (2017) Phil. Trans. R. Soc. A **375**, 20150437.

[8] Harwit M. (2003) Astrophys. J. **597**, 1266.

[9] Elias N. M. (2008) Astron. Astrophys. **492**, 883.

[10] Tamburini F., Thidé B., Molina-Terriza G., and Anzolin G. (2011) Nat. Phys. **7**, 195.

[11] Swartzlander G. A., Ford E. L., Abdul-Malik R. S., Close L. M., Peters M. A., Palacios D. M., and Wilson D. W. (2008) Opt. Express **16**, 10200.

[12] Grier D. G. (2003) Nature **424**, 810.

[13] Padgett M., and Bowman R. (2011) Nat. photon. **5**, 343.

[14] Loke V. L., Asavei T., Parkin S., Heckenberg N. R., Rubinsztein-Dunlop H., and Nieminen, T. A. (2011). Driving optical micromachines with orbital angular momentum in Twisted Photons: Applications of Light with Orbital Angular Momentum, Torres J. P. and Torner L. eds., Wiley, New York.

[15] Piccirillo B., Toscano C., Vetrano F., and Santamato E. (2001) Phys. Rev. Lett. **86**, 2285.

[16] He H., Friese M. E. J., Heckenberg N. R., and Rubinsztein-Dunlop H. (1995), Phys. Rev. Lett. **75** 826.

[17] Ruffner D. B. and Grier D. G. (2012) Phys. Rev. Lett. **108**, 173602.

[18] Mair A., Vazir, A., Weihs G., and Zeilinger A. (2001) Nature **412**, 313.

[19] Fickler R., Lapkiewicz R., Plick W. N., Krenn M., Schaeff C., Ramelow S., and Zeilinger A. (2012) Science **338**, 640.

[20] Gao W. B., et al. (2010) Nat. Phys. **6**, 331.

[21] Dada A. C., Leach J., Buller G. S., Padgett M. J., and Andersson E. (2011) Nat. Phys. **7**, 677.

[22] Brunner N., Cavalcanti D., Pironio S., Scarani V., and Wehner S. (2014) Rev. Modern Phys. **86**, 419.

[23] Wang X. L., et al. (2015) Nature **518**, 516.

[24] Emile O. and Emile J. (2018) J. Adv. Opt. Photon **1**, 157.

[25] Zeng Q., Li T., Song X., and Zhang X. (2016) Opt. Express **2**, 8186.

[26] Duocastella M., and Arnold C. B. (2012) Laser Photon. Rev. **6**, 607.

[27] Nivas J. J., Shutong H., Anoop K. K. , Rubano A., Fittipaldi R., Vecchione A., Paparo D., L. Marrucci L., Bruzzese R., and Amoruso S. (2015) Opt. Lett. **40**, 4611.

[28] Rhodes D. P., Gherardi D. M., Livesey J., McGloin D., Melville H., Freegarde T., and Dholakia K. (2006) J. Modern Opt. **53**, 547.

[29] Olson S. E., Terraciano M. L., Bashkansky M., and Fatemi F. K. (2007) Phys. Rev. A **76**, 061404.

[30] V. Carrat V., Cabrera-Gutiérrez C., Jacquey M., Tabosa J. W., Viaris de Lesegno B., and Pruvost L. (2014) Opt. Lett. **39**, 719.

[31] Tamburini F., Mari E., Sponselli A., Thidé B., Bianchini A., and Romanato F. (2012) New J. Phys. **14**, 033001.

[32] Yan Y., Xie G., P. J. Lavery M. P. J., Huang H., Ahmed N., Bao C., Ren Y., Cao

Y., Li L., Zhao Z., Molisch A. F., Tur M., Miles J. Padgett M. J., and Willner A. E. (2014) Nat. Commun. **5**, 4876.

[33] Wang J., Yang J. Y., Fazal I. M., Ahmed N., Yan Y., Huang H., Ren Y., Yue Y., Dolinar S., Tur M. and, Willner A. E. (2012) Nat. Photon **6**, 488.

[34] Gibson G., Courtial J., Padgett M. J., Vasnetsov M., Pas'ko V., Barnett S. M., and Franke-Arnold S. (2004) Opt. Express **12**, 5448.

[35] Willner A. E., Huang H.,Yan Y., Ren Y., Ahmed N., Xie G., Bao C., Li L., Cao Y., Zhao Z., Wang J., Lavery M. P. J., Tur M., Ramachandran S., Molisch A.F., Ashrafi N., and Ashrafi S. (2015) Adv. Opt. Photon. **7**, 66.

[36] Molina-Terriza G., Torres J. P., and Torner L. (2007) Nat. Phys. **3** , 305.

[37] Yao A. M. and Padgett M. J. (2011) Adv. Opt. Photon. **3**, 161.

[38] Rubinsztein-Dunlop H., Forbes A., Berry M. V., Dennis M. R., Andrews D. L., Mansuripur M., Denz C., Alpmann C., Banzer P., Bauer T. (2016) J. Opt. **19**, 013001.

[39] Padgett M. J. (2017) Opt. Express **25**, 11265.

[40] Erhard M., Fickler R., Krenn M., and Zeilinger A. (2018) Light Sci. Appl. **7**, 17146.

[41] Wang X., Nie Z., Liang Y., Wang J., Li T., and Jia B. (2018) Nanophoton. **7**, 1533.

[42] Padgett M. J. (2014) Proc. R. Soc. A **470**, 20140633.

[43] Siegman A. E. (1990) Lasers (University Science Books, Mill Valley).

[44] van Enk S. J. and Nienhuis G. (1994) J. Mod. Opt. **41**, 963.

[45] Bialynicki-Birula I. and Bialynicka-Birula Z. (2011) J. Opt. **13**, 064014.

[46] Klimov V. V., Bloch D., Ducloy M., and Rios Leite J. R. (2012) Phys. Rev. A **85**, 053834.

[47] Cameron R. P., Barnett S. M., and Yao A. M. (2012) New J. Phys. **14**, 053005.

[48] Zhao Y., Edgar J. S., Jeffries G. D., McGloin D., and Chiu D. T. (2007) Phys.

Rev. Lett. **99**, 073901.

[49] Bliokh K. Y., Dressel J., and Nori F. (2014) New J. Phys. **16**, 093037.

[50] Beijersbergen M. W, Allen L., Van der Veen, H. E. L. O., and Woerdman,J. P. (1993) Opt. Commun. **96**, 123.

[51] Vaity P., Banerji J., and Singh, R. P. (2013) Phys. Lett. A **377**, 1154.

[52] Shutova M., Zhdanova A. A., and Sokolov A. V. (2017) Phys. Lett. A **381**, 408.

[53] Beijersbergen M. W., Coerwinkel R. C. P., Kristensen M., and Woerdman J. P. (1994) Opt. Comm. **112**, 321.

[54] Beniss A., Niemiec R., Brousseau C., Mahdjoubi K., and Emile O. (2013) Proc. Euro. Conf. Antennas Propag. (EuCAP) Gothenburg, Sweden, 8.

[55] Niemiec R., Brousseau C., Mahdjoubi K., Emile O., and Ménard A. (2014) IEEE Antennas Wirel. Prop. Lett. **13**, 1011.

[56] Bazhenov V., Soskin M. S., and Vasnetsov M. V. (1992) J. Mod. Opt. **39**, 985.

[57] Heckenberg N. R., McDuff R., Smith C. P., Rubinsztein-Dunlop H., and Wegener M. (1992) Opt. Quantum. Electron. **24**, S951.

[58] Xiao Q., Klitis C., Li S., Chen Y., Cai X., Sorel M., and Yu S. (2016). Opt. Express **24**, 3168.

[59] Lei T., Zhang M., Li Y., Jia P., Liu G. N., Xu X., Li Z., Min C., Lin J., Yu C., Niu H. and, Yuan X. (2015) Light Sci. Appl. **4**, e257.

[60] Bozinovic N., Yue Y., Ren Y., Tur M., Kristensen P., Huang H., Willner A. E., and Ramachandran S. (2013) Science **340**, 1545.

[61] Khonina S., Kotlyar V., and Soifer V. (1998) Opt. Spectrosc. **85**, 636.

[62] S. Khonina S., Kotlyar V., Skidanov R., Soifer V., Laakkonen P., and Turunen J. (2000) Opt. Commun. **175**, 301.

[63] Kai C., Huang P., Shen F., Zhou H., and Guo Z. (2017) IEEE Photon. J. **9**, 1.

[64] Hariharan P. (2003) Optical Interferometry. 2nd ed. Academic Press, San Diego.

[65] Adhikari R. X. (2014) Rev. Mod. Phys. **86**, 121.

[66] Basistiy V. I., Bazhenov V., Soskin M. S., and Vasnetsov M. V. (1993) Opt. Commun. **103**, 422.

[67] Harris M., Hill C. A., Tapster P. R., and Vaughan J. M. (1994) Phys. Rev. A **49**, 3119.

[68] Soskin M. S., Gorshkov N. V., Vasnetsov M. V., Malos J. T., and Heckenberg N. R. (1997) Phys. Rev. A **56**, 4064.

[69] Shack R.V. (1971) J. Opt. Soc. Am. **61**, 656.

[70] Leach J., Keen S., Padgett M. J., Saunter C., and Love G. D. (2006) Opt. Express **14**, 11919.

[71] Bowman R. W., Wright A. J., and Padgett M. J. (2010) J. Opt. **12**, 124004.

[72] Grunwald R., Elsaesser T., and Bock M. (2014) Sci. Reports **4**, 7148.

[73] Padgett M. J., Arlt J., Simpson N. B., and Allen L. (1996) Am. J. Phys. **64**, 77.

[74] Vickers J., Burch M., Vyas R., and Singh S. (2008) J. Opt. Soc. Am. A **25**, 823.

[75] Chen L., Zhang W., Lu Q., and Lin X. (2013) Phys. Rev. A **88**, 053831.

[76] Osorio C., Molina-Terriza G., and Torres J. (2008) Phys. Rev. A **77**, 015810.

[77] Salakhutdinov V., Eliel E., and Löer W. (2012) Phys. Rev. Lett. **108**, 173604.

[78] Lavery M. P., Speirits F. C., Barnett S. M., and Padgett M. J. (2013) Science **341**, 537.

[79] Lavery M. P., Barnett S. M., Speirits F. C., and Padgett M. J. (2014) Optica **1**, 1.

[80] Emile O. and Emile J. (2017) Opt. Lett. **42**, 354.

[81] Fickler R., Campbell G., Buchler B., Lam P. K., and Zeilinger A. (2016) PNAS **113**, 13642.

[82] Hickmann J. M., Fonseca E. J. S., Soares W. C., and Chávez-Cerda S. (2010) Phys. Rev. Lett. **105**, 053904.

[83] Mourka A., Baumgartl J., Shanor C., Dholakia K., and Wright E. M. (2011) Opt. Express **19**, 5760.

[84] de Araujo L. E. E. and Anderson, M. E. (2011) Opt. Lett. **36**, 787.

[85] Hickmann J. M., Fonseca E. J. S., and Jesus-Silva A. J. (2011) EPL **96**, 64006.

[86] Sillitto R. M. and Sillitto W. (1975) Opt. Acta **22**, 999.

[87] Sztul H. I. and Alfano R. R. (2006) Opt. Lett. **31**, 999.

[88] Emile O. and Emile J. (2014) Appl. Phys. B **117**, 487.

[89] Zhou H., Yan S., Dong J., and Zhang X. (2014) Opt. Lett. **39**, 3173.

[90] Emile O., Le Meur M., and Emile J. (2014) Phys. Rev. A **89**, 013846.

[91] Emile O., Emile J., and Brousseau C. (2014) J. Opt. **16**, 125703.

[92] Fu D., Chen D., Liu R., Wang Y., Gao H., Li F., and Zhang P. (2015) Opt. Lett. **40**, 788.

[93] Zhu J., Zhang P., Fu D., Chen D., Liu R., Zhou Y.,Gao H., and Li F. (2016) Photon. Research **4**, 187.

[94] Liu R., Long J., Wang F., Wang Y., Zhang P., Gao H., and Li F. (2013) J. Opt. **15**, 125712.

[95] Ghai D. P., Senthilkumaran P., Sirohi R. S. (2009) Opt. Lasers Eng. **47**, 123.

[96] Ferreira Q. S., Jesus-Silva A. J., Fonseca E. J., and Hickman J. M. (2011) Opt. Lett. **36**, 3106.

[97] Kumar A., Vaity P., Singh R. P. (2010) Opt. Commun. **283**, 4141.

[98] Guo C. S., Lu L. L., and Wang H. T. (2009) Opt. Lett. **34**, 3686.

[99] Berkout G. C. G. and Beijersbergen M. W. (2008) Phys. Rev. Lett. **101**, 100801.

[100] Shi L., Tian L. and Chen X. (2012) Cin. Opt. Lett. **10**, 120501.

[101] Emile O., Emile J., Viaris de Lesegno B., Pruvost L., and Brousseau C. (2015) EPL **111**, 34001.

[102] Garetz B. A. (1981) J. Opt. Soc. Am. **71**, 609.

[103] Bialynicki-Birula I., and Bialynicka-Birula Z. (1997) Phys. Rev. Lett. **78**, 2539.

[104] Basistiy I. V., Bekshaev A. Y., Vasnetsov M. V., Slyusar V. V., and Soskin M. S. (2002) JETP Lett. **76**, 486.

[105] Speirits F. C., Lavery M. P., Padgett M. J., and Barnett S. M. (2014) Opt. Lett. **39**, 2944.

[106] Arlt J., MacDonald M., Paterson L., Sibbett W., Dholakia K., and Volke-Sepulveda K. (2002) Opt. Express **10**, 844.

[107] Franke-Arnold S., Gibson G., Boyd R. W., and Padgett M. J. (2011) Science **333**, 65.

[108] Korech O., Steinitz U., Gordon R. J., Averbukh I. S., and Prior Y. (2013) Nat. Photon. **7**, 711.

[109] Zhao M., Gao X., Xie M., Zhai W., Xu W., Huang S., and Gu W. (2016) Opt. Lett. **41**, 2549.

[110] Zheng J., Zheng S., Shao Z., and Zhang X. (2018) J Appl. Phys. **124**, 164907.

[111] Gilles H., Cheron B., Emile O., Bretenaker F., and Le Floch A. (2001) Phys. Rev. Lett. **86**, 1175.

[112] Courtial J., Dholakia K., Robertson D. A., Allen L., and Padgett M. J. (1998) Phys. Rev. Lett. **80**, 3217.

[113] Courtial J., Robertson D. A., Dholakia K., Allen L., and Padgett M. J. (1998) Phys. Rev. Lett. **81**, 4828.

[114] Zhou H. L., Fu D. Z., Dong J. J., Zhang P., Chen D. X., Cai X. L., Li F.-L., and Zhang, X. L. (2017) Light Sci. Appl. **6**, e16251.

[115] Zhang W., Gao J., Zhang D., He Y., Xu T., Fickler R., and Chen L. (2018) Phys. Rev. Appl. **10**, 044014.

[116] Mansuripur M., Zakharian A. R., and Wright E. W. (2011) Phys. Rev. A. **84**, 033813.

[117] Beth R. A. (1935) Phys. Rev. **48**, 471.

[118] Beth R. A. (1936) Phys. Rev. **50**, 115.

[119] Carrara N. (1949) Nature **164**, 882.

[120] Allen P. J. (1966) Am. J. Phys. **34**, 1185.

[121] Delannoy G., Emile O., and Le Floch A. (2005) Appl. Phys. Lett. **86**, 081109.

[122] Friese M. E. J., Nieminen T. A., Heckenberg N. R., and Rubinsztein-Dunlop H. (1998) Nature **394**, 348.

[123] Friese M. E. J., Rubinsztein-Dunlop H., Gold J., Hagberg P., and Hanstorp D. (2001) Appl. Phys. Lett. **78**, 547.

[124] Leach J., Mushfique H., di Leonardo R., Padgett M. J., and Cooper J. (2006) Lab Chip **6**, 735.

[125] Pedaci F., Huang Z. X., van Oene M., Barland S., and Dekker N. H. (2011) Nat. Phys. **7**, 259.

[126] Kane B. E. (2010) Phys. Rev. B **82**, 115441.

[127] Franke-Arnold S., Allen L., and Padgett M. J. (2008) Laser and Photon. Rev. **2**, 299.

[128] Emile O. and Emile J. (2016) Opt. Lett., 2016, **41**, 211.

[129] Emile J., Tabuteau H., and Emile O. (2018) Soft Matter **14**, 3829.

[130] Emile O., Brousseau C., Emile J., Niemiec R., Madhjoubi K., and Thidé B. (2014) Phys. Rev. Lett. **112**, 053902.

[131] Emile O., Niemiec R., Brousseau C., Emile J., Mahdjoubi K., Wei W., and Thidé B. (2016) Eur. Phys. J. D **70**, 172.

[132] Emile O., Brousseau C., Emile J., and Mahdjoubi K. (2017) C. R. Phys. **18**, 137.

[133] Demore C. E., Yang Z., Volovick A., Cochran S., MacDonald M. P., and Spalding G. C. (2012) Phys. Rev. Lett. **108**, 194301.

[134] Hefner B. T., Marston P. L. (1999) J. Acoust. Soc. Am. **106**, 3313.

[135] Skeldon K. D., Wilson C., Edgar M., and Padgett M. J. (2008) New J. Phys. **10**, 013018.

[136] Emile O., and Emile J. (2018) Ann. Phys. **530**, 1800111.

[137] Truesdell C. (1968) Essays in the History of Mechanics (Springer-Verlag, Berlin).

[138] Thidé B., Tamburini F., Then H., Someda C. G., Ravanelli R. A. (2014) The

physics of angular momentum radio arXiv:410.4268v3.

[139] Raman C. V. and Bhagavantam S. (1931) Indian J. Phys. **6**, 353.

[140] Torres J. P. and Torner L. (2011) Twisted Photons: Applications of Light with Orbital Angular Momentum (Wiley, New York).

[141] Willner A. E., Wang J., and Huang H. (2012) Science **337**, 655.

[142] Zhou Z. Y., Li Y., Ding D. S., Zhang W., Shi S., Shi B. S., and Guo G. C. (2016) Light Sci. and Appl. **5**, e16019.

[143] Mann, A. (2018) PNAS **115**, 5621.

[144] Edfors O., and Johansson A. J. (2012) IEEE Trans. Anten. Prop. **60**, 1126.

[145] Tamagnone M., Craeye C., and Perruisseau-Carrier J. (2012) New J. Phys. **14**, 118001.

[146] Tamburini F., Thidé B., Mari E., Bianchini A., and Romanato F. (2012) New J. Phys **14**, 118002.